RSC Advances

ROYAL SOCIETY OF CHEMISTRY

www.rsc.org/advances

Eutectic mixture of choline chloride/urea as an assisted-solvent in the synthesis of BiOCl flower-like hierarchical structures with enhanced photocatalytic activity

Jianhua Ge[1], Xuetao Guo[1*], Xin Xu[1], Pingping Zhang[1], Jingling Zhu[1], and Jingbo Wang[2]

(1. School of Earth and Environment, Anhui University of Science & Technology, Huainan 232001

2. Hainan Research Academy of Environmental Sciences, 98 Baiju Avenue, Haikou, Hainan Province, 571126, China)

Abstract: Flower-like BiOCl hierarchical structures were successfully synthesized in the presence of eutectic mixture of choline chloride/urea mixtures through a solvothermal process. The as-prepared sample was characterized by X-ray diffraction (XRD), scanning electron microscopy (SEM), X-ray photoelectron spectroscopy (XPS), N_2 adsorption/desorption analysis, photo-electrochemical analysis and UV-vis diffuse reflectance spectroscopy (DRS). During the reaction process, the eutectic mixtures of choline chloride/urea acted not only as the solvent and the template, but also as a chlorine source for the fabrication of flower-like BiOCl. In addition, the photocatalytic activity toward degradation of RhB in aqueous solution was also investigated. The results showed that the flower-like BiOCl exhibited enhanced photocatalytic activity for the degradation of RhB under sunlight illumination. Meanwhile, the flower-like BiOCl catalyst exhibited without obviously decreases in activity after five cycles. Furthermore, the main reactive species in the catalytic oxidation reaction were detected through radical trapping experiments.

Key words: BiOCl; Eutectic mixture; Solvothermal; Photocatalytic properties

Introduction

The advantages of TiO_2 based photocatalysts have been widely recognized in the past decades. Such as, eliminate contaminants rapidly in water, cheapness, nontoxic

*To whom correspondence should be addressed, Tel: +86554-6668430; Fax: +86554-6668430, E-mail:guoxuetao2005@outlook.com, school of earth and environment, Anhui University of science &technology.

nature, and operation at ambient temperature[1-3]. However, due to its low quantum yields and pure TiO_2 can only be activated by UV-light prevent its wide spread applications. In order to effectively utilize solar energy, the first strategy is to extend modification of TiO_2 by doping, coupling, and sensitization, but it still can not satisfy the requirements for practical application. The other strategy is to develop visible-light-driven photocatalysts[4-5], among semiconductors, BiOCl as efficient photocatalyst to decompose organic pollutants into inorganic substances under sunlight irradiation, have been attracted considerable attentions owing to their open crystalline layered structures and the indirect optical transition, and these results in a high photocatalytic performance [6-9].

As we know, the synthesis method can affect the morphology, size and surface area of the photocatalyst, which decide photocatalytic activity. Hence, the preparation of BiOCl nanoparticles with various morphologies has become a very active research area in recent years [10]. For example, Henle synthesized BiOCl nanoparticles in reverse microemulsions, which is consisting of heptane, nonionic surfactants, and aqueous salt solutions [1]. Deng fabricated single-crystalline bismuth oxyhalides BiOCl nanoplates, nanosheets, and microsheets by using convenient hydrothermal methods [11].

Compared with organic solvents, ionic liquids (ILs) are regarded as “green solvents” due to their low melting point, wide liquid range, negligible vapour pressure and good solubility characteristics and so on [12, 13]. Recently, many different BiOCl hierarchical nano-structure materials have been successfully synthesized in IL. For instance, Xia and his coworkers recently fabricated BiOCl uniform flower-like hollow microsphere and porous nanosphere structures using EG-assisted solvothermal method in the presence of ionic liquid $[C_{16}mim]Cl$ and ionic liquid-PVP system. During the reactive process, ionic liquid not only acted as Cl source but also as solvents and template for the fabrication of BiOCl porous microspheres, exhibited significantly photocatalytic activity [14-16]. However, the high cost of ILs is one of the most important issues hampering their large scale application.

More recently, the mixtures of substituted quaternary ammonium salts, such as choline chloride with urea (carboxylic acids) produce eutectics that are liquid at

ambient temperature and have unusual solvent properties attracted the attention of researchers. Because this type of eutectic mixture that it is sustainable, biodegradable and a large number of variants can be produced from readily available materials. Sheu present the first use of eutectic mixture of choline chloride/malonic acid as a solvent in the synthesis of two metal oxalatophosphates[17, 18].The study shows that the eutectic mixtures plays a vital role in the crystallization of one desired compound. Up to now, little literature makes references to the BiOCl materials synthesized with eutectic mixtures. So, the potential of eutectic solvents in the synthesis of BiOCl remains to be explored.

On the basis of above summarizations, it prompted us to develop a eutectic mixtures-assisted solvothermal method for the synthesis of BiOCl. In this work, flower-like BiOCl hierarchical structures were obtained through a solvothermal synthesis assisted with eutectic mixtures in ethylene glycol mediated conditions. During the process, the eutectic mixtures of choline chloride/urea acted not only as the solvent and the template, but also as chlorine source for the fabrication of flower-like BiOCl. It was found that as-prepared flower-like BiOCl particles exhibited higher photocatalytic activity under sunlight illumination in comparison with plate-like BiOCl particles, which were also synthesized under the same conditions without the presence of eutectic mixtures of choline chloride/urea by using NaCl as the Cl sources.

2. Experimental section

2.1 Materials

All reagents in this experiment were purchased from Aladdin Chemical Regent Co., Ltd (analytical grade) and were used directly without further purification.

2.2 Synthesis of flower-like BiOCl and plate-like BiOCl

Eutectic mixtures of choline chloride/urea were prepared according to the procedure described in the literature[19]. The flower-like BiOCl was synthesized as follows: 0.001 mmol of $Bi(NO_3)_3.5H_2O$ was dissolved in 20 mL ethylene glycol solution under magnetic stirring at room temperature, being followed by dissolution of 10 mmol eutectic mixtures into the above solution. After continuously stirring for 30 min, and was transferred into 30 mL teflon-lined stainless steel autoclave up to

80% of the total volume. Subsequently, the autoclave was then heated at 140℃ for 24h in a static state.The resulting white solid particles were separated and successively washed with water and alcohol, and dried at 50℃ in vacuum for 24h. For comparison, the plate-like BiOCl particles were also synthesized under the same conditions without the presence of eutectic mixtures of choline chloride/urea by using NaCl as the Cl sources.

2.3 Characterization

The crystal structure of the samples was recorded by X-ray diffractometer (XRD, Bruker D8 ADVANCE) using Cu-Kα X-ray source (λ=0.15418 nm). While Infrared (FT-IR) spectra were recorded on Tensor 27(BrukerT27) equipment in the 4000-400 cm^{-1} range. X-ray photoelectron spectroscopy (XPS) measurements were accomplished in a Thermo ESCALAB 250 instruments (USA) using nonmonochromatic Al Ka(hv = 1486.6 ev) radiation. Morphologies of BiOCl was carried out with a scanning electron microscope (SEM, JEOL JSM-6510LV), which was operated at an acceleration voltage of 10 kV. Photo-electrochemical analysis was characterized on a CHI660E workstation in a standard three-electrode configuration with 0.5 M Na_2SO_4 solution as the electrolyte. The ultraviolet-visible light (UV-Vis) spectra of BiOCls were recorded on UV-2450 spectrophotometer (Shimadzu Corporation, Japan). The N_2 adsorption and desorption isotherms were performed at 196 ℃ on an ASAP 2020 (Micromeritics USA). Prior to measurements, the sample was degassed at 120 ℃ for 10 h. The specific surface area was determined from the linear part of the BET equation (P/P_0 =0.05–0.25). The pore size distribution was derived from the desorption branch of the N_2 isotherm using the Barrett–Joyner–Halenda (BJH) method.

2.4 Photocatalytic activity measurement

Photocatalytic properties of the prepared BiOCl were valuated in terms of the degradation of RhB. The photodegradation experiments were performed in a slurry reactor containing a solution of RhB (200mL, 10 mg/L) and photocatalyst. A Xe lamp was used as a sunlight source. Prior to irradiation, the suspension was kept in the dark under strongly magnetically stirring for 30 min to ensure the establishment of an

adsorption/desorption equilibrium. At given time intervals, about 8 mL aliquots were collected from the suspension and centrifuged immediately, and the concentration of RhB after illumination was determined by checking the absorbance at 553nm using a UV-Vis spectrophotometer.

3 Results and discussion

3.1 XRD analysis

The crystal structure and phase purity of the as-synthesized BiOCl samples were first characterized by X-ray diffraction. As shown in Fig.1, it was found that all the identified peaks for flower-like BiOCl and plate-like BiOCl can well be indexed to the tetragonal structure of BiOCl (JCPDS No. 06-0249).The major X-ray diffraction peaks at 2θ values of 12.06°, 25.95°, 32.50° and 33.67° correspond to the (001), (011), (110) and (102) crystalline planes of BiOCl. It could be found that no other peak corresponding to the Bi_2O_3 or $BiCl_3$ were detected [20]. Thus, this important result indicated that all the products are composed of a single phase BiOCl with high purity.

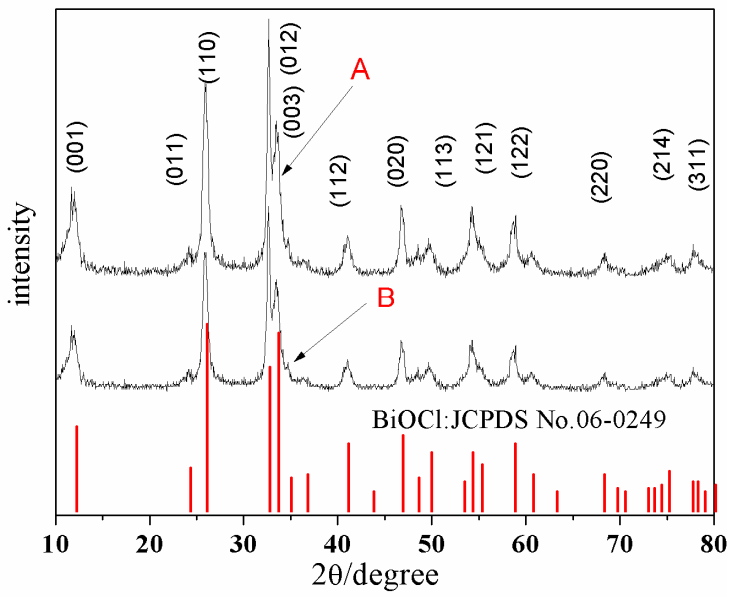

Fig.1 XRD patterns of BiOCl synthesized (A: flower-like BiOCl;B: plate-like BiOCl)

3.2 XPS analysis

To investigate the states of the ions and the composition of the BiOCl was examined using XPS.The survey XPS Spectrum (Fig.2a) suggests that the sample

contains only the elements of Bi, O, C and Cl, and the carbon peak came from the adventitious carbon on the surface of the sample. it can be seen that two strong peaks with binding energy of 158.9 eV and 164.05 eV ,as displayed in Fig.2a, are for the Bi 4f 7/2 and Bi 4f 5/2 region for BiOCl, respectively. Meanwhile the peak binding energies of 529.5 eV , shown in Fig.2c,was assigned to O1s.On the other hand, the Cl2p peak, shown in Fig.2d, is deconvoluted into two peaks (198.2, 200.2 eV), which are assigned, respectively [15,21].

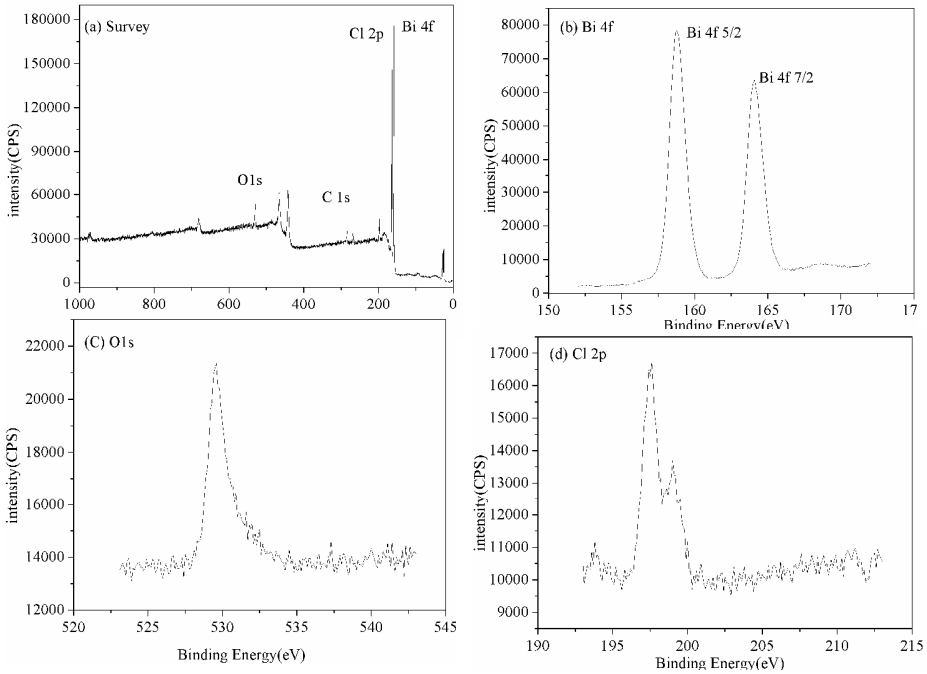

Fig.2 XPS spectra of the flower-like BiOCl.(a) Survey of the sample; (b) Bi 4f; (c) O 1s; (d) Cl 2p.

3.3 SEM analysis

SEM images were taken in order to observe microstructures of the BiOCl photocatalysts in detail. Fig.3(a,b) show typical SEM images of the as-prepared BiOCl samples in the presence of eutectic mixture of choline chloride/urea mixtures through a solvothermal process. With the SEM images characterized, it could clearly demonstrates that the morphologies of the samples are flower-like hierarchical structures, with an average diameter of 1-2 μm, and the sizes are uniform, which are assembled by a large number of BiOCl nanosheets. For the purpose of comparison,

BiOCl samples were also prepared through a solvothermal process by using NaCl as the Cl source without eutectic mixture of choline chloride/urea mixtures (Fig.3c,d). It is found that the BiOCl prepared with NaCl is sphere-like or flake-like in structure. Moreover, the Fig.3b displays that the entire flower-like BiOCl hierarchical structures are composed of BiOCl nano-plates on the surface, different from the BiOCl microspheres synthesized without eutectic mixture of choline chloride/urea mixtures. Therefore, aside from being the Cl source, eutectic mixture of choline chloride/urea mixtures is also acted as a soft template and a stabilizer, inducing the growth of BiOCl flower-like hierarchical structures.

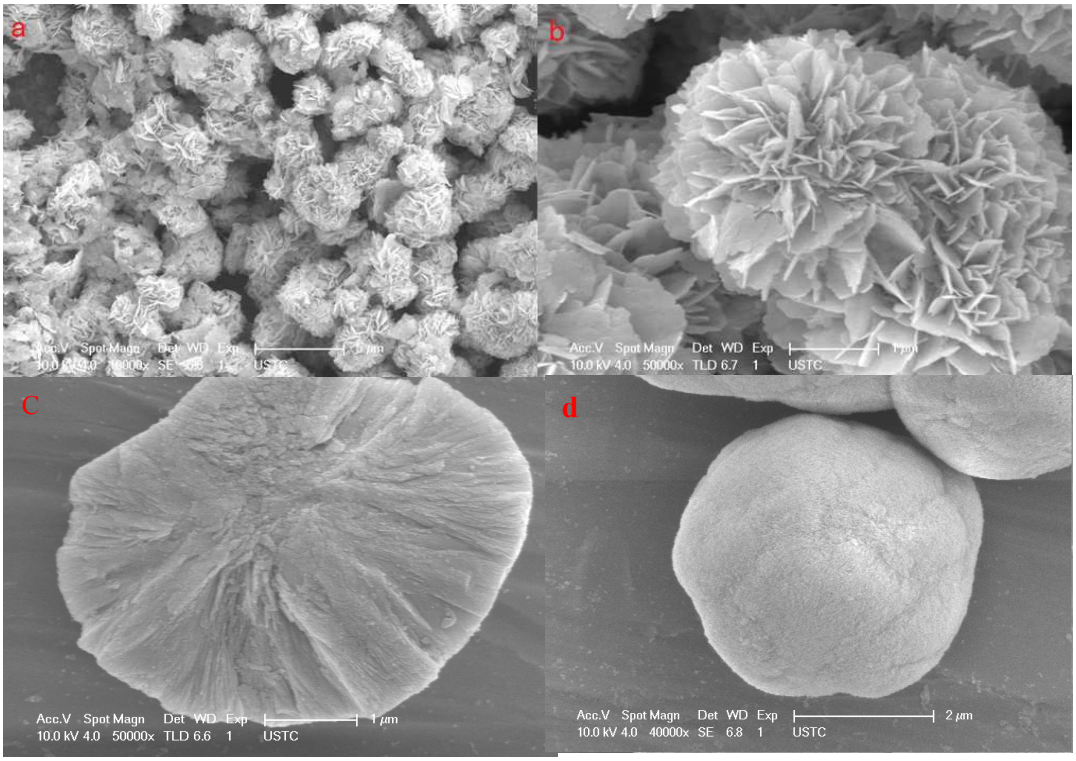

Fig.3 SEM images of the BiOCl photocatalyst

On the basis of the above characterizations, the possible mechanism on formation of flower-like BiOCl (Fig.4) might be divided into three steps:(1) the formation of BiOCl and their growth into flake-like in structure at the early stage; (2) these primary BiOCl nanosheets to form loose flower-like microspheres in the presence of eutectic mixture of choline chloride/urea mixtures; (3) the formation of flower-like BiOCl regular hierarchical microspheres through a

dissolution-recrystallization process of the preformed nanoparticles. The detailed formation mechanism of flower-like BiOX in the presence of eutectic mixture of choline chloride/urea mixtures through solvothermal process needs further investigation.

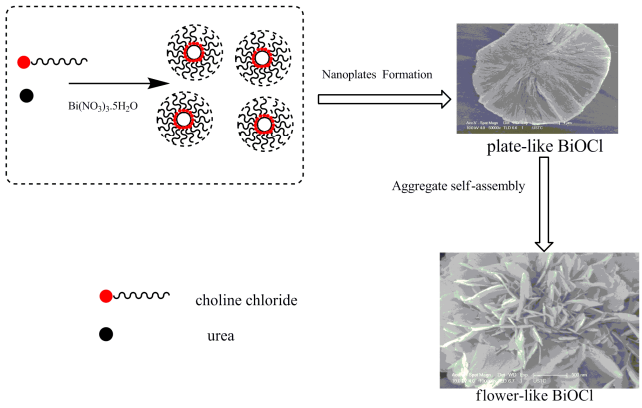

Fig.4 Schematic illustration of proposed formation mechanism of flower-like BiOCl

3.4 Optical absorption properties of BiOCl

The optical properties of flower-like BiOCl was studied by UV–Vis diffuse reflectance spectroscopy. Fig.5A is the typical UV-Vis diffuse reflectance spectroscopy of BiOCl flower-like structures. Due to the band-gap transition, the prepared BiOCl samples indicated an obvious increase in absorption with wavelengths lower than about 350 nm. A classical Tauc approach was further employed to estimate the E_g value of the BiOCl crystals, the energy intercept of a curve of $(ahv)^2$ vs hv yields E_g for a direct transition [22]. As shown in Fig.5, the band gap of BiOCl flower-like hierarchical structures synthesized in the presence of eutectic mixture of choline chloride/urea mixtures was calculated to be 3.05 eV, which was behind the plate-like BiOCl (3.35eV) and the Degussa TiO_2 (3.2eV).This result supported that BiOCl with flower-like hierarchical structures have suitable band gap to be activated by visible-light for photocatalytic decomposition of organic contaminants. Thus, it can make the photocatalytic process more efficient compare with the plate-like BiOCl and the Degussa TiO_2.

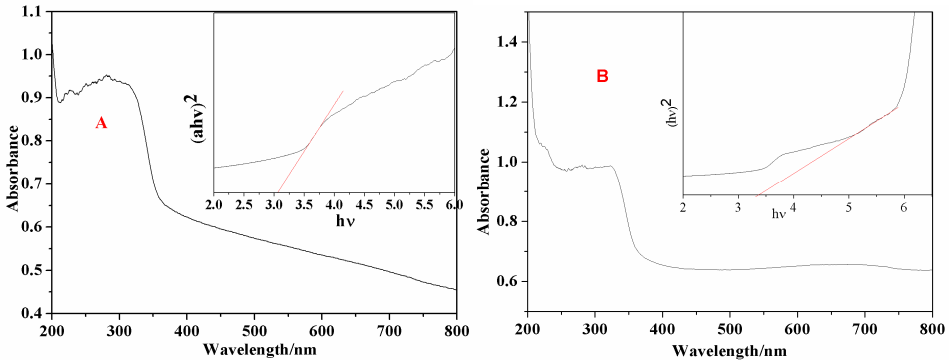

Fig 5.UV-vis diffuse reflectance spectra and $(ahv)^2$ vs hv curve of BiOCl (A: flower-like BiOCl;B: plate-like BiOCl)

3.5 Nitrogen adsorption/desorption analysis

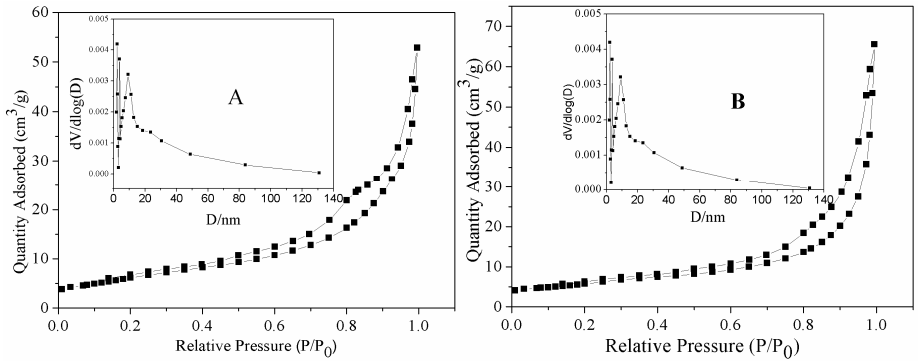

Fig. 6 N_2 adsorption-desorption isotherms and corresponding pore size distribution curves (inset) (A: flower-like BiOCl;B: plate-like BiOCl)

The N_2 adsorption/desorption isotherms together with the corresponding pore size distribution of the flower-like BiOCl and plate-like BiOCl were shown in Fig.6. It could be observed that both the flower-like BiOCl and plate-like BiOCl exhibited type IV curves according to the IUPAC nomenclature with two hysteresis loops in the relative pressure range of 0.4–1.0, implying bimodal pore-size distributions in the mesoporous and macroporous region[2]. The first hysteresis loop at a low relative pressure (0.4–0.8), corresponding to the intra-aggregated pores of BiOCl crystals. The second hysteresis loop at a high relative pressure (0.8–1.0), corresponding to the larger pores that could be formed between secondary particles due to the aggregation of nanosheets into flower-like hierarchical architectures. The surface area are calculated to be as high as about 26.79 $m^2.g^{-1}$and 20.38 $m^2.g^{-1}$ for the flower-like

BiOCl and plate-like BiOCl samples, respectively.

3.6 Photocatalytic properties

Firstly, the photocatalytic activities of the flower-like BiOCl were evaluated by degradation of RhB in aqueous solution under sunlight irradiation as a test reaction. As shown in Fig.7. It is displayed that the intensity of the absorption peak of RhB is decreased gradually with the irradiation time increasing, accompanied with a blue-shift of the main absorption peak (~553 nm), indicating the photoinduced degradation of RhB. It is also found that the process of photocatalytic degradation can be divided into two stages. In the first stage, the RhB is firstly adsorbed on the surface of BiOCl due to its high specific surface area and then transferred into its actived state (RhB*) under sunlight irradiation, thus the adsorption efficiency became the dominant factor. At second stage, electrons were injected from the actived RhB into the conduction band of the flower-like BiOCl catalyst, and then electron was trapped by molecular oxygen subsequently. During this stage, photocatalysis efficiency is the controlling factor. In a word, the flower-like BiOCl served as RhB absorber and electron-transfer medium in this photocatalytic process. Therefore, the flower-like structure of BiOCl catalyst with high surface area could absorb many RhB and active species on its surface, which could enhance its photocatalytic activities.

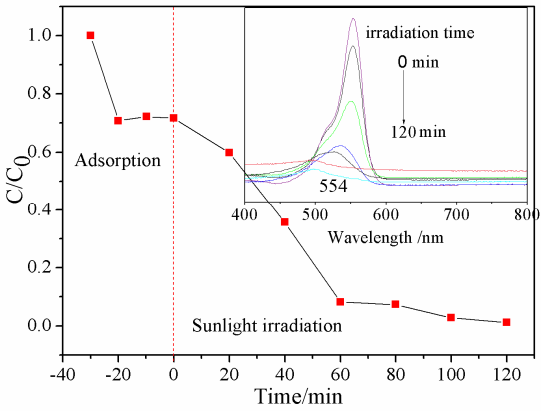

Fig.7 the photocatalytic properties of the flower-like BiOCl

As a comparison, RhB degradation with BiOCl photocatalyst using plate-like BiOCl and commercial photocatalyst p25 were also performed. As shown in the Fig.8, the photocatalytic activities of the flower-like BiOCl is much higher than that of

plate-like BiOCl photocatalyst and p25. The photodegradation efficiency of RhB by flower-like BiOCl could reaches 98.5% after 75 min reaction. Interestingly, 84.7%, 65.2% of RhB is photocatalytically degraded by plate-like BiOCl and p25, respectively. This is because the flower-like BiOCl possesses plenty of pores between nanoplates, which can contribute to the transport the RhB molecules to get to the active sites. In addition, the intermeshed nanoplates on the surface of the flower-like BiOCl wall and hollow interior cavity can allow multiple reflections of visible light, which enhances light-harvesting and thus increases the quantity of photogenerated electrons and holes available to participate in the photocatalytic decomposition of RhB.

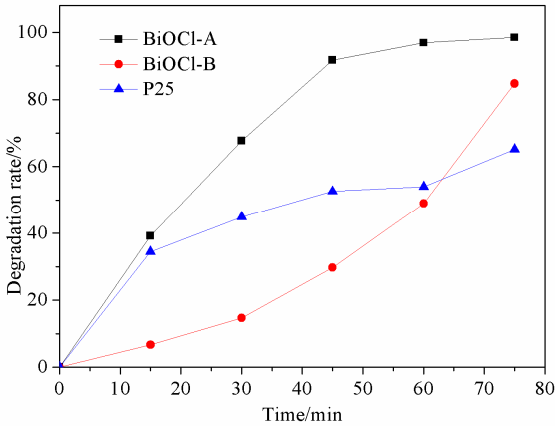

Fig.8 degradation profile of RhB over different BiOCl (A: flower-like BiOCl;B: plate-like BiOCl and P25)

The photocatalytic properties of the flower-like BiOCl with hierarchical structures were further studied by photocurrent experiment, a unique method to confirm the efficient separation of photogenerated carriers in the photocatalytic system. Fig.9 displays the photocurrent densities of flower-like BiOCl under sunlight irradiation where the photocurrent was measured at open circuit potential in 0.5 M Na_2SO_4 aqueous solution. The current densities of the flower-like BiOCl as a function of time were recorded by switching sunlight ON/OFF with durations of 50s. Photocurrents of the flower-like BiOCl rapidly decrease to zero as soon as the light is turned off and recover when the light is turned on, reflecting the movements of photo-generated electrons.

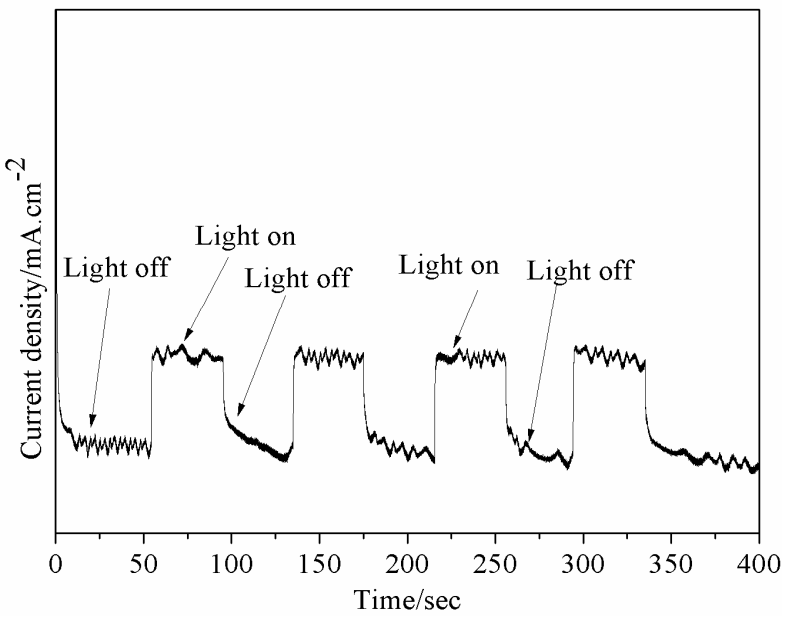

Fig.9 photoelectrochemical chronoamperometry results for flower-like BiOCl

3.7 Possible photocatalytic oxidation mechanism

With aim to elaborate the photodegradation of RhB mechanism in the present of flower-like BiOCl photocatalysts, the main reactive species in the catalytic oxidation reaction were detected through radical trapping experiments. The scavengers used in this experiment are ammonium oxalate (AO) for h^+, isopropanol (IPA) for •OH and N_2 for $•O^{2-}$, respectively [23]. Effects of a series of scavengers on the RhB conversion over the flower-like BiOCl are shown in Fig.10. The photocatalytic conversion of RhB decreases significantly from98.6 % to 10.8% after adding N_2, indicating $•O^{2-}$ is the main active species in the photocatlytic oxidation process, and when AO are added, the photocatalytic conversion of RhB decreases to 96.5% and 17.4%, respectively, which indicates h^+ also play an important role in the photocatlytic oxidation of RhB. In summary, the results indicated that the dominating reactive species involved in the photocatalytic degradation of RhB in aqueous solution are $•O^{2-}$ and h^+.

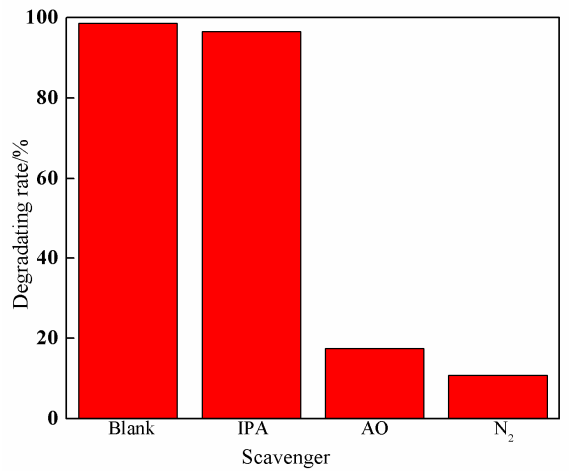

Fig.10 effect of different scavengers on the degradation of RhB

3.8 Reusability of the flower-like BiOCl

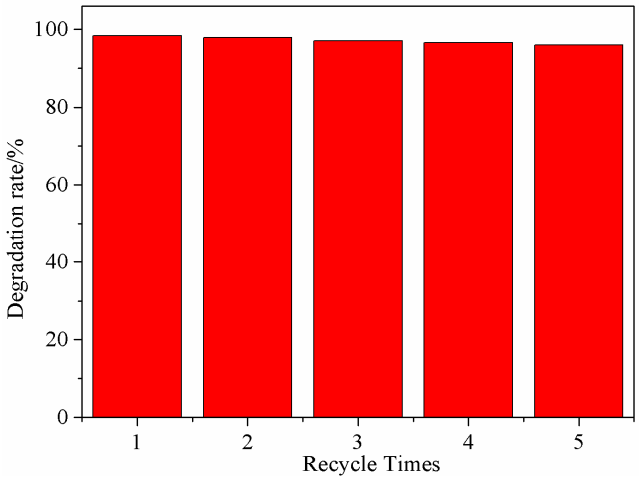

Fig. 11 The photodegradation of RhB in solution for 5 cycles using flower-like BiOCl

It is well known that the stability of photocatalysts is a vital concern for practical application[24-27]. The reusability of lower-like BiOCl was evaluated by repeating photodegradation of RhB under identical conditions, after each photocatalytic degradation reaction, the flower-like BiOCl could be separated by centrifugalization from solution system easily, washed with deionized water, and dried at 80℃before the next run. As shown in Fig.11, the flower-like BiOCl catalyst exhibited without obviously decrease in activity after five cycles of photodegradation of RhB, highlighting the stability and reusability of the flower-like BiOCl. Meanwhile, as shown in Fig.12, there was no obvious difference between the FT-IR spectra of the

flower-like BiOCl and the recycle flower-like BiOCl, and the SEM images of the recycle BiOCl photocatalyst exhibited flower-like hierarchical structures(Fig.13), which indicates that the flower-like structure of BiOC has not been changed after five cycles of photodegradation of RhB.

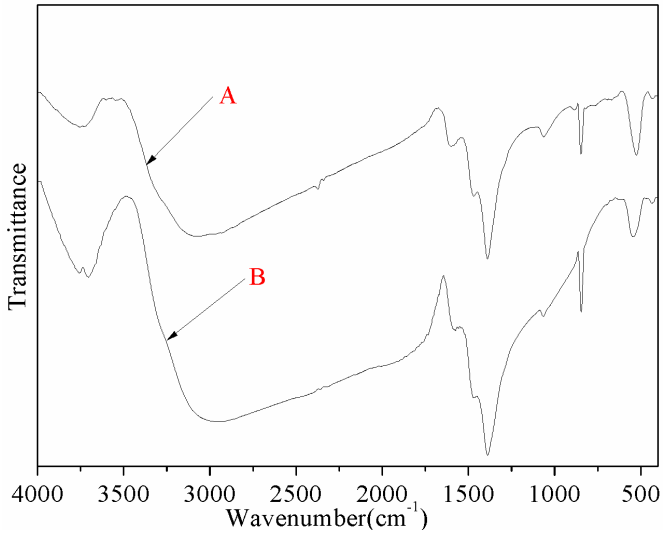

Fig.12 FT-IR spectra of the BiOCl (A: flower-like BiOCl;B: recycle BiOCl)

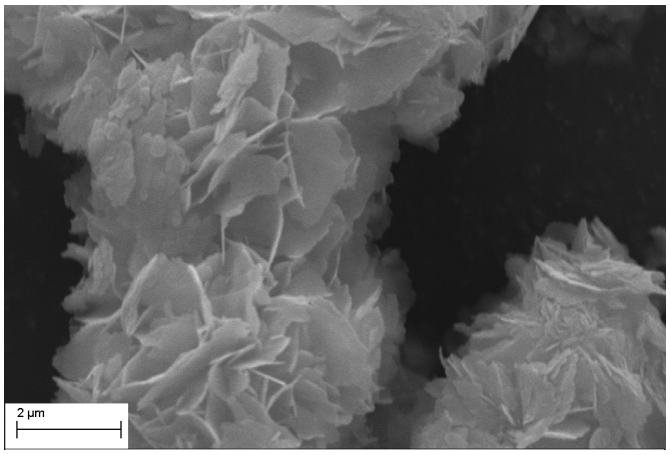

Fig.13 SEM images of the BiOCl photocatalyst after 5 recycle

Conclusions

We have demonstrated a method for synthesising flower-like BiOCl photocatalyst in the presence of eutectic mixture of choline chloride/urea through a solvothermal process. The flower-like BiOCl fabricated by this process exhibited enhanced photocatalytic properties toward the degradation of RhB in comparison with plate-like BiOCl particles,

which were also synthesized under the same conditions without the presence of eutectic mixtures of choline chloride/urea by using NaCl as the Cl sources and p25. During the reaction process, the eutectic mixtures of choline chloride/urea acted not only as the solvent and the template, but also as a chlorine source for the fabrication of flower-like BiOCl. The uniformly distributed flower-like BiOCl generally having average diameter of 1-2 μm, and the sizes are uniform, which are assembled by a large number of BiOCl nanosheets, and the band gap of flower-like BiOCl was calculated to be 3.05 eV. Moreover, investigation of photocatalytic oxidation mechanism revealed that the dominating reactive species involved in the photocatalytic degradation of RhB in aqueous solution are $\bullet O^{2-}$ and h^{+}. Meanwhile, the flower-like BiOCl catalyst exhibited without obviously decreases in activity after five cycles. Furthermore, we expect that this new system can pave the way for the purposive synthesis of other nanosized photocatalysts with high photocatalytic activity.

Acknowledgements

This work was supported by the Natural Science Foundation of Universities of Anhui Province(KJ2014A069), Postdoctoral Science Foundation of Anhui Province (2013DG125)and Natural Science Foundation of Hainan Province (414194).

References

1. J. Henle, P. Simon, A. Frenzel, S. Scholz and S. Kaskel, *Chemistry of Materials*, 2007, **19**, 366-373.
2. Z. Zhang, Y. Zhou, Y. Zhang, S. Xiang, S. Zhou and X. Sheng, *RSC Advances*, 2014, **4**, 7313-7320.
3. L. Ye, J. Liu, Z. Jiang, T. Peng and L. Zan, *Applied Catalysis B: Environmental*, 2013, **142-143**, 1-7.
4. X. Shen, L. Zhu, N. Wang, L. Ye and H. Tang, *Chem Commun (Camb)*, 2012, **48**, 788-798.
5. N. Zhang, Y. Zhang and Y. J. Xu, *Nanoscale*, 2012, **4**, 5792-5813.
6. L. Ye, Y. Su, X. Jin, H. Xie and C. Zhang, *Environmental Science: Nano*, 2014, **1**, 90-112.
7. X. Zhang, Z. Ai, F. Jia and L. Zhang, *Journal of Physical Chemistry C*, 2008, **112**,

747-753.

8. J. Jiang, K. Zhao, X. Xiao and L. Zhang, *Journal of the American Chemical Society*, 2012, **134**, 4473-4476.

9. M. Guan, C. Xiao, J. Zhang, S. Fan, R. An, Q. Cheng, J. Xie, M. Zhou, B. Ye and Y. Xie, *Journal of the American Chemical Society*, 2013, **135**, 10411-10417.

10. H. F. Cheng, B. B. Huang and Y. Dai, *Nanoscale*, 2014, **6**, 2009-2026.

11. H. Deng, J. Wang, Q. Peng, X. Wang and Y. Li, *Chemistry – A European Journal*, 2005, **11**, 6519-6524.

12. C. M. Gordon, J. D. Holbrey, A. R. Kennedya and K. R. Seddonb, *J. Mater. Chem.*, 1998, **8**, 2627-2636.

13. C. M. Gordon, *Applied Catalysis A: General*, 2001, **222**, 101-117.

14. J. X. Xia, S. Yin, H. M. Li, H. Xu, L. Xu and Q. Zhang, *Colloids and Surfaces a-Physicochemical and Engineering Aspects*, 2011, **387**, 23-28.

15. J. X. Xia, S. Yin, H. M. Li, H. Xu, L. Xu and Y. G. Xu, *Dalton Transactions*, 2011, **40**, 5249-5258.

16. J. Xia, J. Zhang, S. Yin, H. Li, H. Xu, L. Xu and Q. Zhang, *Journal of Physics and Chemistry of Solids*, 2013, **74**, 298-304.

17. A. P. Abbott, D. Boothby, G. Capper, D. L. Davies and R. K. Rasheed, *Journal of the American Chemical Society*, 2004, **126**, 9142-9147.

18. C.Y. Sheu, S.-F. Lee and K.H. Lii, *Inorganic chemistry*, 2006, **45**, 1891-1893.

19. A. P. Abbott, G. Capper, D. L. Davies, R. K. Rasheed and V. Tambyrajah, *Chemical communications (Cambridge, England)*, 2003,**1**, 70-71.

20. S. Wu, C. Wang, Y. Cui, T. Wang, B. Huang, X. Zhang, X. Qin and P. Brault, *Materials Letters*, 2010, **64**, 115-118.

21. C. Wang, C. Shao, Y. Liu and L. Zhang, *Scripta Materialia,* 2008, **59**, 332-335.

22. K. Zhang, C. Liu, F. Huang, C. Zheng and W. Wang, *Applied Catalysis B: Environmental*, 2006, **68**, 125-129.

23. W. Liu, M. L. Wang, C. X. Xu, S. F. Chen and X. L. Fu, *Journal of Molecular Catalysis A-Chemical*, 2013, **368**, 9-15.

24. X. Wang, S. Li, H. Yu, J. Yu and S. Liu, *Chemistry-a European Journal*, 2011, **17**,

7777-7780.

25. R. H. Waldemer, P. G. Tratnyek, R. L. Johnson and J. T. Nurmi, *Environmental Science & Technology*, 2007, **41**, 1010-1015.

26. W.S. Wang, H. Du, R.X. Wang, T. Wen and A.W. Xu, *Nanoscale*, 2013, **5**, 3315-3321.

27. F. Song, Y. Ding, B. Ma, C. Wang, Q. Wang, X. Du, S. Fu and J. Song, *Energy & Environmental Science*, 2013, **6**, 1170-1184.